Available online at www.sciencedirect.com
ScienceDirect
Tectonophysics 437 (2007) 37–50
TECTONOPHYSICS
www.elsevier.com/locate/tecto

Shear zones in porous sand: Insights from ring-shear experiments and naturally deformed sandstones

Anita Torabi [a,*], Alvar Braathen [a], Fabrice Cuisiat [b], Haakon Fossen [a]

[a] Centre for Integrated Petroleum Research, Department of Earth Science, University of Bergen, Post Box 7800, 5020 Bergen, Norway
[b] Norwegian Geotechnical Institute, Post Box 3930, N-0806 Oslo, Norway

Received 20 September 2006; received in revised form 15 February 2007; accepted 27 February 2007
Available online 19 March 2007

Abstract

We have used thin section and particle size analyses to relate stress–strain relationships in ring-shear experiments with burial depth at the time of faulting in naturally deformed samples. We show that the burial depth (level of stress) and the amount of shear displacement at the time of deformation are important factors influencing the type of grain breakage and also the type of shear zone that forms. Further, petrographic image analyses with porosity estimations show systematic change related to progressive development of the shear zones and the development of two end-member types of shear zones: (a) Shear zones with diffuse boundaries formed at low levels of stress, and (b) Shear zones with sharp boundaries formed at higher levels of stress. We consider the mechanism of deformation at shallow depth/low level of stress to be dominated by reorganization, rolling and flaking of grains. This mechanism causes rough surfaces of the grains at the margins and within the shear zones. At greater depths or at higher levels of stress, the predominant mode of fracturing transgresses from flaking to grain splitting, resulting in lower porosity values and greater particle size reduction. Furthermore, this transition results in a slow increase in the power law dimension from 1.4 to 1.6 with respect to the increased displacement.

Keywords: Shear zone; Stress; Strain; Particle size; Porosity; Burial depth

1. Introduction

Zones of localized deformation found in highly porous rocks and sediments, in most cases mechanically stronger and with lower porosity than surrounding rocks, are commonly referred as deformation bands (Aydin et al., 2006; Fossen et al., in press). In this study we investigate a type of deformation band which has a strong component of shear and involves both compaction and shearing of sand and sandstone. Shear deformation is localized to a zone, which we will call a shear zone. It is commonly seen that the petrophysical properties of the rock are changed during the course of the deformation. In particular, the permeability within the shear zone may change dynamically during and after deformation, dependent on many factors. Their occurrence and formation have therefore been the subjects of considerable attention among petroleum and hydro geologists.

Initiation and development of shear zones as deformation structures in highly porous, granular rock are affected by the mechanical and hydraulic properties of the host rock. These properties depend on the microstructural evolution of the rock, in particular the mechanical processes that act during fault formation, how these processes interact, and the stage of evolution

* Corresponding author.
E-mail address: anita.torabi@cipr.uib.no (A. Torabi).

0040-1951/$ - see front matter © 2007 Elsevier B.V. All rights reserved.
doi:10.1016/j.tecto.2007.02.018

(Ngwenya et al., 2003). Outcrop and drill core observations represent only the final results of deformation. Indirect information about the evolution of the structures can be gained by studying natural structures representing various stages of strain. Alternatively, such information can be directly obtained through controlled laboratory experiments performed in a deformation apparatus, such as the ring-shear apparatus.

The mechanism of deformation in porous sand and sandstones is dependent on the initial porosity, grain size, pore fluid pressure, temperature, burial depth, and state of stress and strain throughout the deformation history (Fossen et al., in press). These factors control the type of shear zone that forms and influence its thickness. For example, high porosity and coarse grain size combined with shallow burial depth (low confining pressure) at the time of faulting tend to increase the thickness of shear zones (e.g. Antonellini and Aydin, 1999).

The deformation mechanism controlling factors are conveniently isolated and studied in the laboratory. Hence the advantage of experimental study of shear zones in granular materials is well documented. Such studies have attracted significant attention from geologists, rock and soil mechanics engineers, and geophysicists alike (Mandl et al., 1977; Zhu and Wong, 1997; Zhang and Tullis, 1998; Mair and Main, 2000; Main and Mair, 2001; Mair and Fyre, 2002; Sperrevik et al., 2002; Lothe et al., 2002; Garga and Sendano, 2002; Clausen and Gabrielsen, 2002; Kjelstad et al., 2002; Ngwenya et al., 2003; Agung et al., 2004; Sassa et al., 2004). Most works are based on triaxial and uniaxial compressional tests. However some of the studies, including Mandl et al. (1977), Zhang and Tullis (1998), Garga and Sendano (2002), Sperrevik et al. (2002), Clausen and Gabrielsen (2002), Agung et al. (2004) and Sassa et al. (2004) used a low stress ring-shear apparatus. Mandl et al. (1977) used the ring-shear apparatus to study the development of shear zones and the accompanying changes in texture and stress state in granular material at a maximum of 920 kPa. Agung et al. (2004) investigated the evolution of shear zone structure in undrained ring-shear tests at 180 kPa under different shear displacements.

In the present study the occurrence and development of shear zones in sand has been investigated using a new high-stress ring-shear apparatus designed and built at the Norwegian Geotechnical Institute (NGI, Oslo, Norway). This instrument can handle up to 20 MPa imposed normal stresses, corresponding to about 2 km or more of overburden. Our aim is to explore the formation of shear zones and associated porosity change inside deformed sample at the simulated condition of relatively shallow burial depth. We implement the experimental results in the interpretation and classification of natural shear zones. Our outcrop samples are from an in-house database on faulted sandstones in Sinai (Egypt), Corsica (France), and Utah (USA). In the light of burial depth for the study areas at the time of deformation we studied and compared the results of experiments and natural rocks in order to further understand the physical processes of faulting. This has been performed by microstructural study of deformed sand and sandstones based on comparison of thin sections from experiments and from natural rocks.

2. Ring-shear apparatus

The ring-shear device was originally designed to study the residual strength of soils (Hvorslev, 1939; Bishop et al., 1971). In the ring-shear apparatus, the sample is forced to shear along a predefined plane located at the separation of the upper and lower confining rings (Hvorslev, 1939). Later Mandl et al. (1977) used the ring-shear apparatus to study shear zones in granular material. For a good historical review of the ring-shear apparatus and further information, the reader is referred to Sassa et al. (2004). The effect of clay and sand properties, strain rate and geometrical aspects on the clay smear continuity in the fault zone has been studied by Sperrevik et al. (2002) and Clausen and Gabrielsen (2002), both performing their experiments at NGI. Limitations inherent

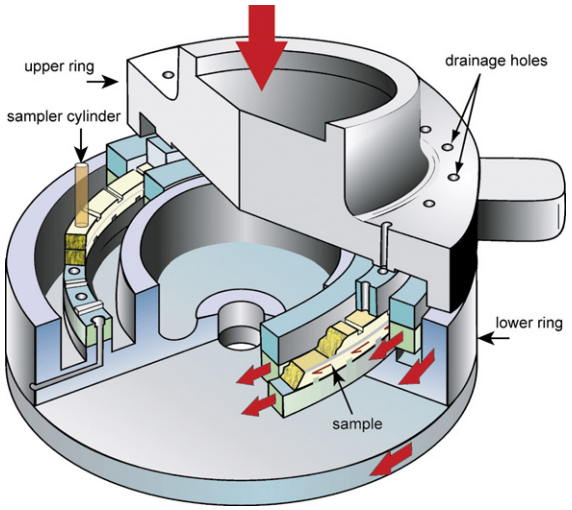

Fig. 1. A simplified sketch of the ring-shear cell. Rotating parts are drawn in light blue and movable parts in grey. The material sample is yellow. The horizontal red arrows on the lower ring indicate direction of movement. The vertical red arrow on the top of the upper ring shows the direction of loading on the ring-shear cell. Notice the drainage points placed on the upper and lower rings and knives to transfer shear stress to the sample. The width of the ring specimen is 25.4 mm and its height is 45 mm. The area of the sample is equal to 223 cm^2. The diameter of sampler cylinder is 1 in. Courtesy of NGI.

in the previous ring-shear apparatus at NGI (i.e. low stress level used for geotechnical applications) have motivated the construction of a new ring-shear device (Fig. 1). The new ring-shear apparatus can handle up to 20 MPa normal stresses, simulating more than 2 km burial depth, thus representing a significant improvement over the previous one. Besides, thin sections prepared from final samples can be used for porosity measurements and particle size analysis and further in the analysis of deformation under different stress conditions.

The ring-shear apparatus operates as a uniaxial deformation device during normal loading prior to shearing (similar to Mandl et al., 1977). During the rotation in the Mandl ring-shear apparatus, the normal loading remains constant but the maximum principal stress rotates due to shear stress such that at the horizontal shear zone the angle between the shear zone and the normal stress is equal to 45° (see Mandl et al., 1977).

The ring-shear apparatus consists of five parts (Cuisiat and Skurtveit, 2006):

- The ring-shear assembly and reaction frame
- The loading system
- The shearing system
- The hydraulic system
- Instrumentation, data acquisition and control systems

The ring-shear assembly consists of a pedestal, upper and lower frames, upper and lower rings, and inner and outer confining rings. The sample is contained within the annular space created between the inner and outer confining rings, and the lower and upper rings. The width of the annular space between the rings is 25.4 mm. The maximum height of the sample is 45 mm, limited by the need for seating of the O-rings at the upper ring to ensure hydraulic sealing. The area of the sample is equal to 223 cm^2. On the upper and lower rings, 48 knives (or grooves) are evenly located to ensure transfer of the torque to the specimen. 48 openings for valves are evenly distributed between the knives at the upper and lower rings for flow measurements. During shearing, the upper ring is fixed and only the lower ring rotates clockwise. Two reaction arms on the upper frame provide the reaction forces against the rotation forces of the lower assembly. Two load cells measure the reaction forces, which in the absence of friction are equal to the shear forces exerted on the specimen.

The following variables are measured during an experiment:

- Vertical force from MTS (MTS is a registered trademark) load cell (F_{MTS})
- Lateral forces F1 and F2 from tangential load cells
- Stroke from MTS transducer (δ_{MTS})
- Axial displacement from internal LVDT, i.e. Linear Variable Differential Transformer, (δ_{LVDT})
- Absolute motor rotation, torque, rotation velocity
- Pore pressures at upper and lower GDS (Global Digital System Ltd.) pumps (u_{up}, u_{low})
- Pressure difference across sample from pressure transducer (Δu)
- Status of automatic valves (open/closed)

The following variables are calculated and logged during an experiment:

- Shear stress τ : $\tau = \dfrac{2(F_1 + F_2)R}{\pi(r_o + r_i)(r_o^2 - r_i^2)}$

  where R is the radial distance between lateral load cells, r_o is the outer radius of the test specimen and r_i is the inner radius of the specimen; F_1, F_2 are the lateral forces from tangential load cells.
- Normal stress σ : $\sigma = \dfrac{F_{MTS}}{\pi(r_o^2 - r_i^2)}$

  where F_{MTS} is the vertical force from the MTS machine;
- Shear displacement at mid-sample l : $l = 2\pi \dfrac{(r_o + r_i)}{2} \dfrac{\theta}{360}\theta$

  is the rotation angle of the lower ring in degrees.

3. Ring-shear sample description and testing procedures

The test program was designed for initial testing of the apparatus and to explore its potential for studying sand deformation. In total, four different types of sand have been used (Table 1). Three types of sand from

Table 1
Description of sands used in the ring-shear experiments

Type of sand	Grain size (D_{60}) in mm	Age	Type	Angularity	Location
Bornholm no. 1	0.4	Jurassic	Quartzarenite	Subrounded–subangular	Denmark
Bornholm no. 17	0.2	Jurassic	Quartzarenite	Subrounded–subangular	Denmark
Bornholm no. 15	0.93	Early Jurassic	Quartzarenite	Subrounded–subangular	Denmark
Baskarp	0.17	Holocene	Quartzarenite	Subangular–angular	Sweden

Bornholm, Denmark (Jurassic) and a Holocene, well-sorted sand from Baskarp, Sweden were used for the low stress experiments. The Baskarp sand was also used for the high-stress experiments. The sands contain more than 90% quartz and have different grain size and angularity. The Bornholm sand was chosen because of its sub-rounded form and availability in different grain sizes at NGI. We have performed drained experiments at atmospheric pore pressure, and the shear rate was so slow that any induced overpressure would not exceed 100 kPa at any time during shearing. This value is small compared to the total normal stress applied on the specimen (5 or 20 MPa), which ensures that the shear induced pressure build-up will not influence the frictional behavior of the sands. Testing procedures for the new ring-shear apparatus were developed during the experimental program (Cuisiat and Skurtveit, 2006).

- The silt fraction (>0.075 mm) of the material was removed prior to mounting of the sample because of potential clogging of the filters by fine material.
- Sand was tamped into the cell in a wet condition. The amount of water needed varies with the type of sand, the mixture should be sticky, not a slurry.
- The lower ring was filled with sand. The top surface was flattened with a flat knife.
- First the sample was saturated with water. The experiments were then carried out in drained conditions (outlet opened to atmosphere).
- The sample was then loaded normally with a rate of 1 MPa/min until the desired normal stress was reached.

In tests RT04, RT05, RT06, RT08, RT09, RT10, RT13; a vertical cyclic load at 28 kN was applied (100 cycles: mean: 28 kN, amplitude: 5 kN, frequency: 0.05 Hz) to ensure full penetration of the "knives" into the sample, and homogeneous stress distribution within the sample.

- Minimum rest period was 15 min before shearing.
- The shearing has been done stepwise with stops for flow measurements under constant normal stresses (shear rate was 2°/min). Flow measurement was done before every stage of shearing.
- Thin section samples were collected with a steel cylinder at the end of the tests. The steel cylinder was pushed down vertically into the sample (perpendicular to the shear zone) from top to the bottom without lateral movement. The samples were oven-dried at 105°C for 24 h and then impregnated with epoxy under vacuum. A detailed description of the tests is presented in Table 2.

4. Methodology of analyzing the thin sections

Polished thin sections from sheared sand and sandstones have been prepared and studied by both optical and Scanning Electron Microscope (SEM). Backscattered Electron Images (BSE) from the SEM were generated from thin sections and analyzed by means of standard image analysis software (ImageJ). Particle size area distributions based on grain areas were obtained from the BSE Images. The selected areas in pixels were calibrated in square millimeters by setting the real scale on the image.

The description of the particle size distribution for the samples includes statistical analysis. The latter is presented as exceedence frequency plots for all the thin sections. Exceedence Frequency (EF) of a particular value of a measured variable is defined as the number of data with values greater than that value, divided by the total number of the data.

Table 2
Description of the ring-shear experiments

Test no.	Sand type	Grain size (D_{60}) in mm	Initial porosity (%)	Porosity reduction due to loading	Initial height (mm)	Vertical stress (MPa)	Rotation (degree)	Shear displacement (mm)
RT01	21 Bornholm	0.373	44.6	2.9	40	5	45	109.75
RT02	21 Bornholm	0.373	45	3.3	40	5	60	146.34
RT03	21 Bornholm	0.373	45	3.3	40	5	75	182.93
RT04	21 Bornholm	0.373	45	4	44	5	360	878.07
RT05	17 Bornholm	0.191	47.5	2.4	40	5	60	146.34
RT06	15 Bornholm	0.934	43.4	6.8	44	5	150	365.86
RT08	Baskarp	0.176	37	1.7	45	5	450	1097.6
RT09	Baskarp	0.176	41	4.1	44	20	75	182.93
RT10	Baskarp	0.176	41	5.4	44	20	45	109.75
RT13	15 Bornholm	0.934	43	3.5	44.5	5	75	184.06

In the present study, the plots of log EF versus log particle size areas have been investigated. The best fit for a given particle size distribution of a shear zone is a power law described by its dimension D (exponent). The calculated D is two-dimensional but can be converted to three dimensions by simply adding 1 (Sammis et al., 1987; Blenkinsop, 1991).

Porosity has been measured in thin sections through binary images from BSE images (Table 3). However, since porosity measurements are influenced by the threshold level between black (pores) and white (particles) pixels, and any void appears black in the binary images, the measured porosities may be slightly overestimated.

5. Results from ring-shear experiments

Based on the detailed analysis of the thin sections from the ring-shear experiments we have classified the shear zones into two different categories:

i) Shear zones with diffuse boundaries formed at low level of stress.
ii) Shear zones with sharp boundaries formed at higher levels of stress.

This division is supported by particle size analysis using high-resolution 2-D images (BSE images) from thin sections. In this context, it is important that the distributions and not the averages of particle sizes are indicative of the underlying processes of cataclastic deformation (Marone and Scholz, 1989). At a low level of stress (5 MPa normal stress), flaking of the grains is the dominant mode of deformation (Fig. 2a), resulting in rough grain surfaces. At higher levels of stress (20 MPa normal stress), the grains mostly break by splitting (Fig. 2b). Changing of the dominant grain breakage mode from flaking to splitting creates different types of shear zones. Based on thin section studies, vertical sections through the deformed sand have been separated into three main parts (Fig. 3a),

- The "top layer", representing the upper part.
- The "shear zone" or the middle part.
- The "bottom layer" or the lower part of the section.

The boundaries of the shear zones are for the most part gradual in the thin sections for experiments performed at 5 MPa normal stress and low rotations (shear displacements); such as for thin sections from experiments RT01, RT02, RT03, RT06 and RT13. We call such shear zones *diffuse boundary shear zones* (Fig. 3a). However, in some thin sections, such as RT04, RT08 and RT09, RT10; sharp shear zone boundaries are visible at high shear rotation (high displacements) under 5 MPa normal stresses. They are also present for the relatively lower shear strain displacements obtained under 20 MPa normal stresses. The margins of such *sharp boundary shear zones* are here named the "upper" and "lower shear zone margin", respectively (Fig. 3b). The diffuse boundary shear zones are wider than the sharp boundary shear zones. RT09 (20 MPa; 75 degree rotation) represents the best example of

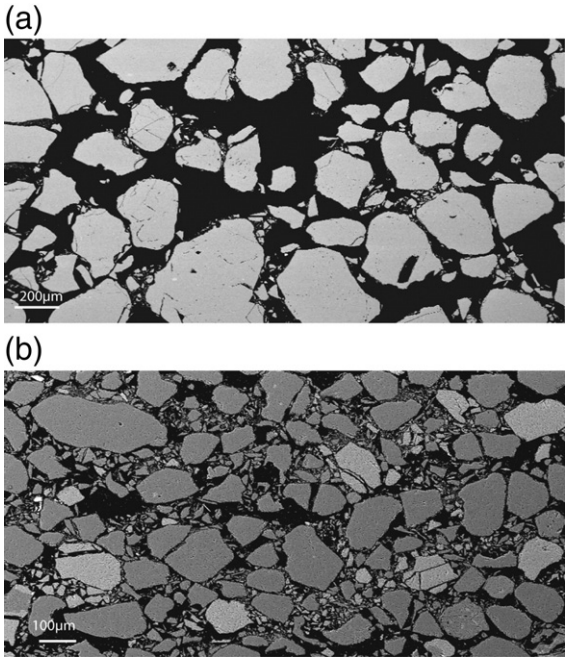

Fig. 2. Different types of grain breakage in thin sections; (a) grain flaking is dominant at low level of stress (BSE image from RT01, top layer); (b) grain splitting is the dominant mechanism at higher levels of stress (BSE image from RT09, top layer).

Table 3
Estimated porosities from BSE images of thin sections from ring-shear experiments

Test no.	Initial porosity (%)	Top layer porosity (%)	Upper margin shear zone porosity (%)	Shear zone porosity (%)	Lower margin shear zone porosity (%)	Bottom layer porosity (%)
RT01	44.6	42	–	33	–	–
RT02	45	39	–	23		
RT03	45	40	–	20		
RT04	45	32	20	15	18	30
RT06	43.4	35		24		31
RT08	37	34	31	11	29	30
RT09	41	24	20	13	15	25
RT10	41	18	9	7	11	28
RT13	43	32		15		36

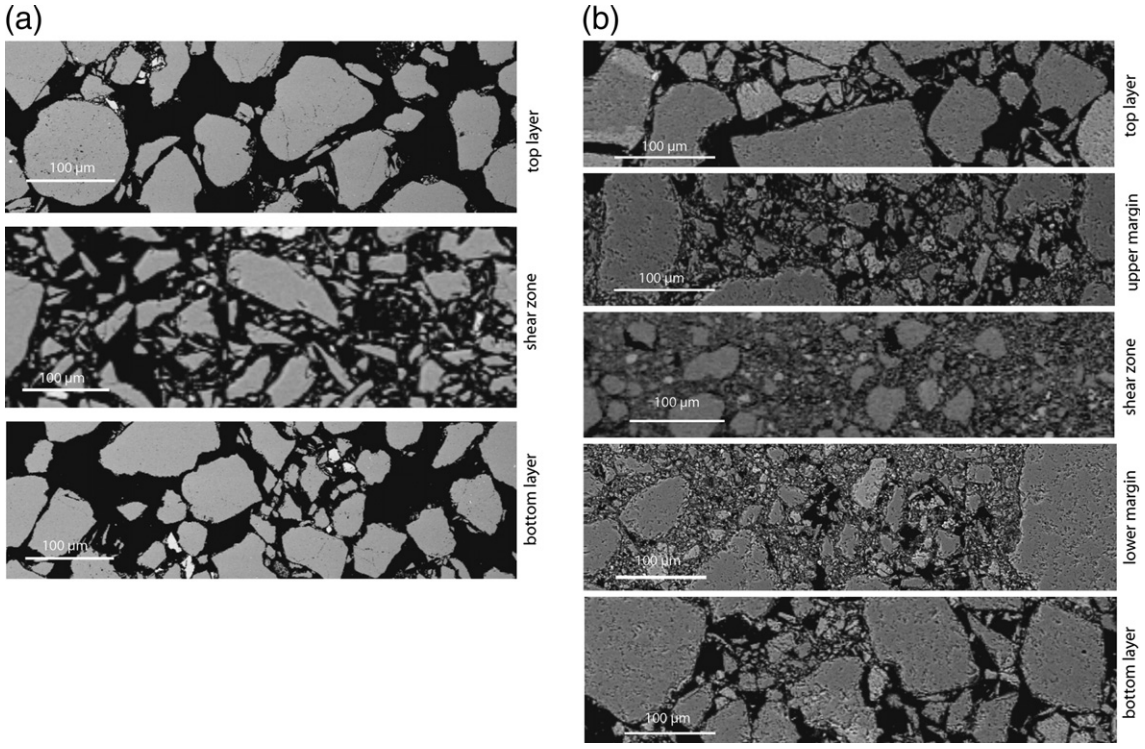

Fig. 3. Classification of shear zones based on BSE images from SEM study; (a) note the formation of a diffusive boundary shear zone at low level of stress, seen in an example from RT02 and (b) sharp boundary shear zone at high level of stress, seen in an example from RT09.

a strongly layered shear zone. This shear zone shows a more compacted central part with maximum reduction in particle size and significant porosity decrease (Figs. 3b and 4a, b). The shear zone is surrounded by margins and the top and bottom layers that contain coarser particle size compared to the shear zone. In sharp boundary shear zones like RT09 there is an asymmetry in the particle size distribution, with slightly more particles size reduction in the lower than the upper margin. Similar observations have been reported by Mandl et al. (1977) and Agung et al. (2004) for layered shear zones.

The particle size distribution plots for sample RT09 (Fig. 4b) indicate that the best fit to the particle size distribution is a power law with a low D value (1.44). The overall results reveal that increasing the normal stress and/or shear stress (by rotation) changes the D values gradually from 1.4 at low levels of stress to 1.5 at higher levels of stress. Based on the results of the experiments, we have chosen to explore three variables, namely the role of shear displacement, grain size and loading.

5.1. The role of shear displacement

Four experiments have been conducted on the pure, medium-grained, sub-rounded Bornholm sand at 5 MPa. The experiments involved different amounts of rotation (shear displacement, Fig. 5a). With increasing shear displacement, the shear stress rose up to yield strength, which is the start of dominant grain fracturing between 2.3–2.7 MPa for these experiments. The post-yield development was in two parts, with an early (low-strain) history of gentle increase in shear stress and general shear localization (seen in RT01, RT02, RT03, RT04, Fig. 5a) before the shear stress started to increase faster (as seen in RT04 in Fig. 5a). Fig. 5b illustrates that the porosity change during the rapid increase of shear stress (up to 2.7 MPa) is very small. In the first part of the post-yield evolution porosity decreased faster than in the second part (only observed in RT04). This change indicates the onset of strong shear localization in the sand. The irregularities in the curves in Fig. 5a and b are probably related to uneven penetration of the knives into the specimen to transfer shear stress. The analysis of particle size distribution of thin sections from RT01, RT03, and RT04 reveals progressively more particle size reduction with increasing shear strain (displacement), see Fig. 6. The shear zones in the first three tests (RT01, RT02, and RT03) can be classified as shear zones with diffuse boundaries. The

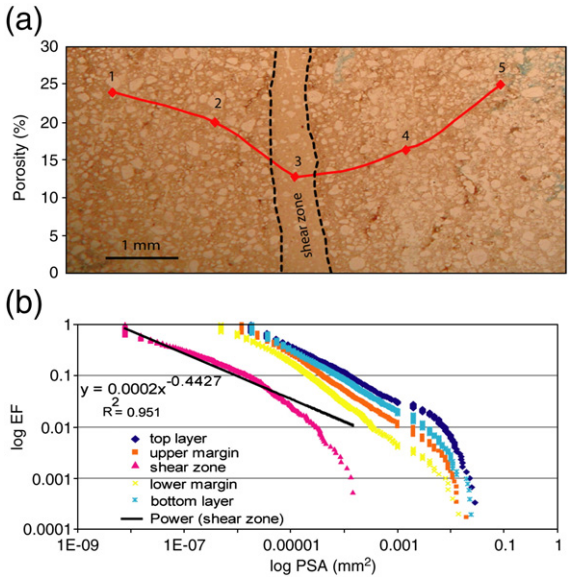

Fig. 4. Sharp boundary shear zone in an example from RT09; (a) Porosity variation inside the sample presented on the petrographic image; the maximum reduction occurred in the middle of the shear zone (point 3); points 1 and 5 show approximate locations of top and bottom layers and points 2 and 4 show locations in upper and lower margins. (b) Particle size analysis of the sample RT09, which shows EF (exceedence frequency) versus PSA (particle size area). Note the particle size reduction from outside the shear zone towards the middle of the shear zone. The shear zone is well layered and classified as a sharp boundary shear zone. A power law fit represents the best fit on the curve with 95% confidence.

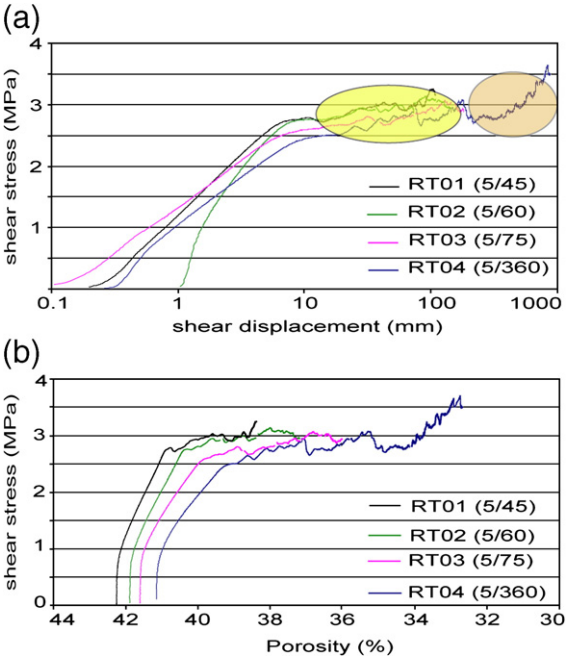

Fig. 5. (a) Shear stress versus shear displacement for RT01, RT02, RT03, RT04, which illustrate that with increasing shear displacement, shear stress rises up to yield strength (start of the grain crushing at 2.3–2.7 MPa). The post-yield has two parts, the first part has a gentler slope (yellow ellipse) than the second part (brown ellipse); the numbers in parentheses refer to normal stress in MPa, and rotations in degrees respectively. (b) Porosity is approximately constant in pre-yield part of the experiments. The porosity reduction is faster in the first part of the post-yield field.

shear zone in RT04 can be interpreted as a sharp boundary shear zone.

5.2. Effect of grain size

The ring-shear dataset enables the comparison of sands with different grain sizes, since the sands employed vary from medium-grained Bornholm sand in RT01, RT02, RT03, and RT04 via coarse-grained Bornholm sand in RT06 and RT13 to fine-grained Bornholm sand in RT05 (Table 1). Comparison of the results from experiments RT01, RT02, RT03, RT04, RT05, RT06, and RT13 shows no significant change in the frictional coefficient (ratio of shear stress to normal stress) of the sands with change in grain size at 5 MPa normal stresses; they show similar behavior for comparable shear displacements (Fig. 7a). However, *increasing* the degree of rotation from test to test makes significant differences in the final grain size distribution. Similarly, when comparing particle sizes of RT03 and RT13, which were both run at 5 MPa and 75 degree rotation (i.e. 182.93 mm shear displacement), the results show similar grain size reduction for two different grain sizes (Fig. 7b). Both of the shear zones can be defined as having diffuse boundaries.

5.3. Effect of loading

Normal stress prior to rotation creates irreversible deformation due to compaction of the sand (Fig. 8a).

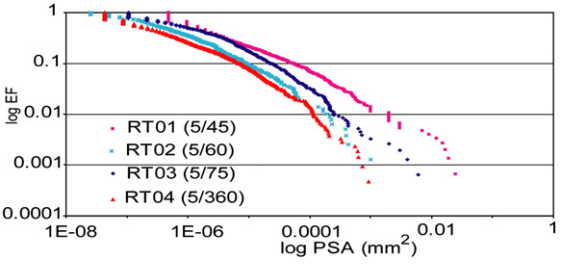

Fig. 6. Particle Size Area (PSA) versus Exceedence Frequency (EF) for shear zone samples from RT01 (45 degree, rotation), RT02 (60°), RT03 (75°), RT04 (360°), all loaded to 5 MPa but experiencing increased rotation. The plot shows how increased rotation reduces the particle size systematically. The numbers in parentheses refer to normal stress in MPa, and rotation in degrees respectively.

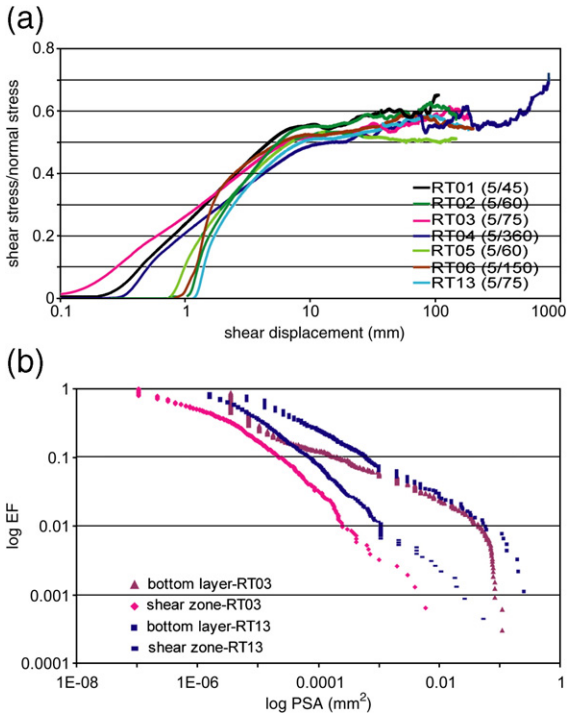

Fig. 7. (a) Friction coefficient as a function of shear displacement for coarse (sample from RT06 and RT13), medium (RT01, RT02, RT03, RT04), and fine (RT05) grained Bornholm sand. The plots suggest similarity in friction coefficient for experiments run at 5 MPa. (b) Particle size analysis for samples from RT03 (medium Bornholm sand) and RT13 (coarse Bornholm sand) both deformed at 5 MPa normal stress. They show a similar distribution of the particle size reduction for the two tests. The numbers in parentheses refer to normal stress in MPa, and rotation in degrees respectively.

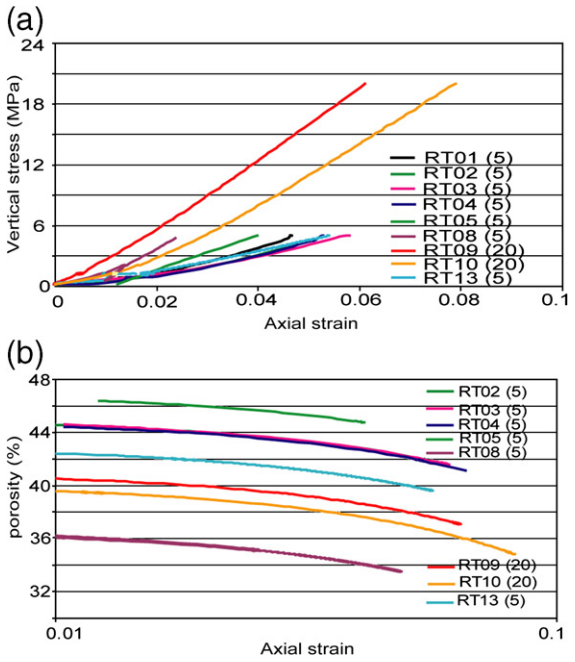

Fig. 8. (a) Effect of initial loading, all the experiments show compaction of the sand at the loading stage. (b) Effect of loading on porosity for all samples; with increase in axial strain the porosity decreases as a result of compaction. The numbers in parentheses refer to normal stress in MPa.

Furthermore, compilation of all of the experiments (Fig. 8b) shows that with increasing axial strain during normal loading prior to shearing, the porosity decreases, thus confirming compaction during normal loading. Once rotation is imposed and shear displacement starts to accumulate in the post-yield stage, fracturing becomes more pronounced. Comparison of the test RT08 (5 MPa, 450 degree rotation) with RT09 (20 MPa, 75 degree rotation) and RT10 (20 MPa, 45 degree rotation), all run on fine-grained Baskarp sand (Fig. 9), show that at higher (20 MPa) normal stress, the yield strength increases to more than 10 MPa, and the shear zone becomes more localized. With further increase in shear displacement, the shear stress declines in RT09 and RT10. Test RT08, on the contrary, shows a pronounced peak in its yield strength, which can be related to lower, imposed normal stress (5 MPa) and low initial porosity. This is in accordance with Kjelstad et al. (2002), who showed the effect of initial porosity on the behavior of the same type of sand in direct shear experiments. Further, RT08 shows that after reaching the yield strength, the shear stress drops to a stable level (residual strength), see Fig. 9.

6. Examples of natural shear zones

Small shear localizations that form as a result of compaction and shear in porous rocks in nature are

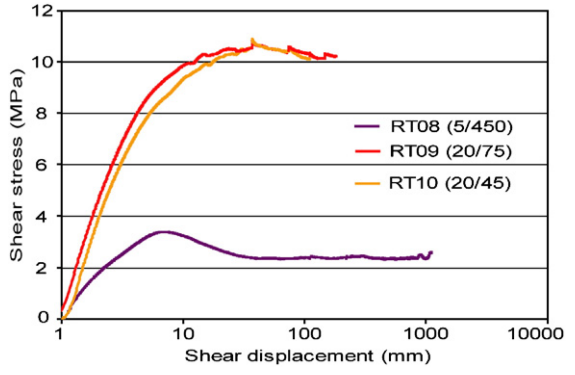

Fig. 9. Shear strength increases at higher normal stresses, comparison between tests RT09, RT10 (20 MPa) and RT08 (5 MPa), all run on fine-grained Baskarp sand. The numbers in parentheses refer to normal stress in MPa, and rotation in degrees respectively.

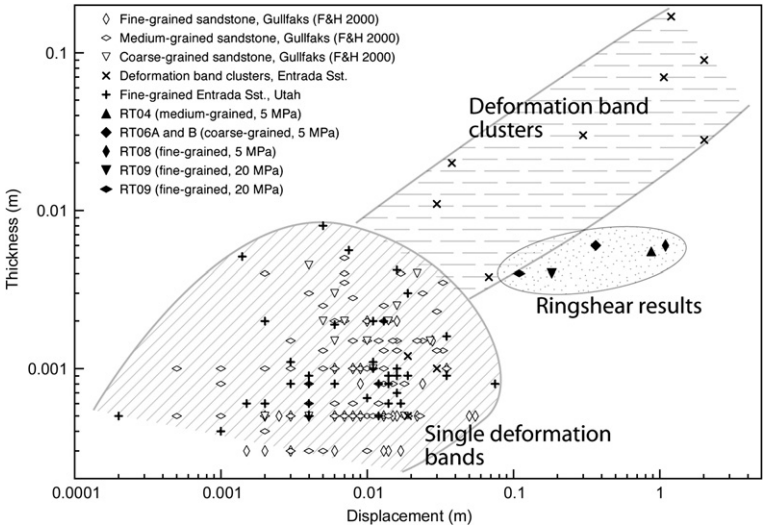

Fig. 10. Thickness and displacement relationship for natural deformation bands and experimental shear zones; the shear zones from ring-shear experiments show approximately similar thickness but higher displacement than the natural single deformation bands, in this sense they are similar to the deformation band clusters. Data from Gullfaks are from Fossen and Hesthammer (2000).

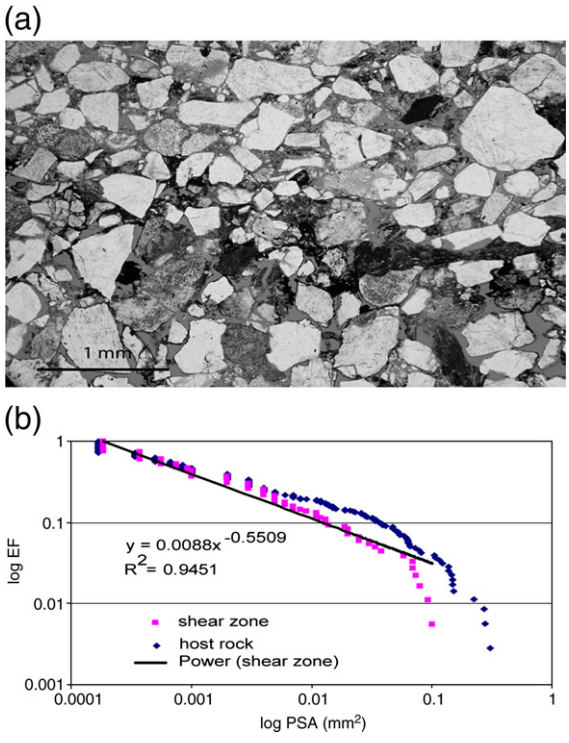

Fig. 11. (a) Petrographic image of the shear zone from thin section Corsica-3 (France). Note that, owing to the extensive flaking, the shear zone is classified as diffuse boundary shear zone. (b) Particle size analysis of the sample, which shows particle size reduction in the shear zone. The power-law fit to the shear zone particle size distribution has a low *D* value.

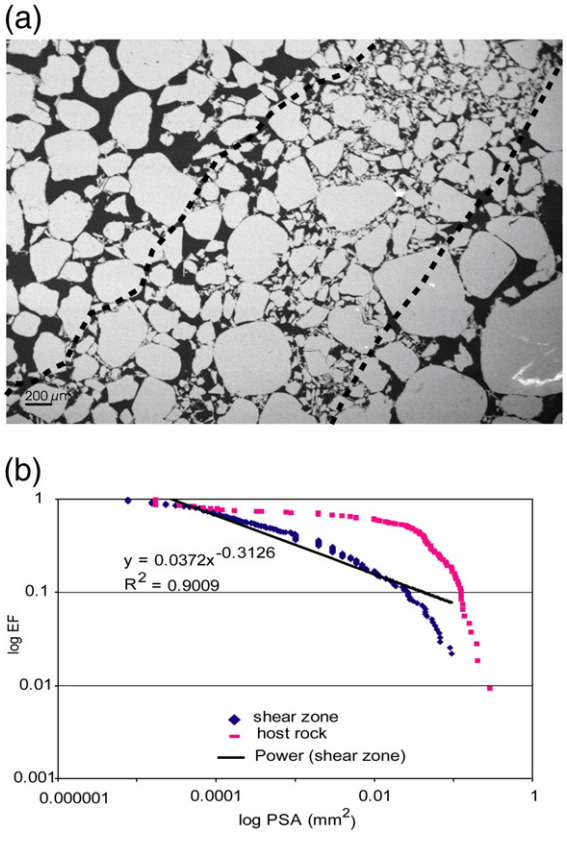

Fig. 12. (a) BSE image from thin section TM-4 (Sinai, Egypt). Note both flaking and splitting of the grains; the shear zone is classified as diffuse boundary shear zone. (b) Particle size analysis of the sample, which shows particle size reduction in the shear zone. The power-law fit to the shear zone particle size distribution has a low *D* value.

called deformation bands (Aydin, 1978) or, more specifically, compactional shear band (Schultz and Siddharthan, 2005; Fossen et al., in press). They have been studied throughout the world (e.g., Underhill and Woodcock, 1987; Fowles and Burley, 1994; Antonellini and Aydin, 1999; Antonellini and Aydin, 1999; Fossen and Hesthammer, 2000; Lothe et al., 2002; Rawling and Goodwin, 2003). Comparison of natural deformation bands with the experimental shear zones presented here reveals that they have a similar mm- to cm-scale range in thickness (Fig. 10). On the other hand, most natural examples have maximum displacements of a few centimeters, while created shear zones in ring-shear apparatus have up to 100 cm displacement.

We have studied samples from faulted, porous sandstones collected from Sinai (Egypt), Corsica (France), and Utah (USA). Most deformation bands in the database are not easily comparable with the experimental shear zones, however, there are similarities that are useful to highlight in a comparison. The differences can for example be ascribed to the occurrence of cement that is found in most reservoir sandstones. In order to avoid the effect of cement, which is absent in the experiments, the degree of cementation is small or negligible in the selected samples. Three thin sections were selected as examples due to good similarity with experimental shear zones. Thin section Corsica-3 shows a deformation band in poorly consolidated, shallow marine, medium-grained sandstone, sampled in the damage zone of a normal fault in the Aleria basin (Corsica, France). The sand is composed mainly of quartz, some feldspar and rock fragments. The throw of the band is about 5 mm, and was formed at a maximum burial depth of about 100 m. Thin sections TM-4 and WK-7 show deformation bands in a medium-grained fluvial sandstone sampled in the damage zone of the Tayiba Fault in Nubian Sandstone (eastern Suez Rift, Egypt) (Beach

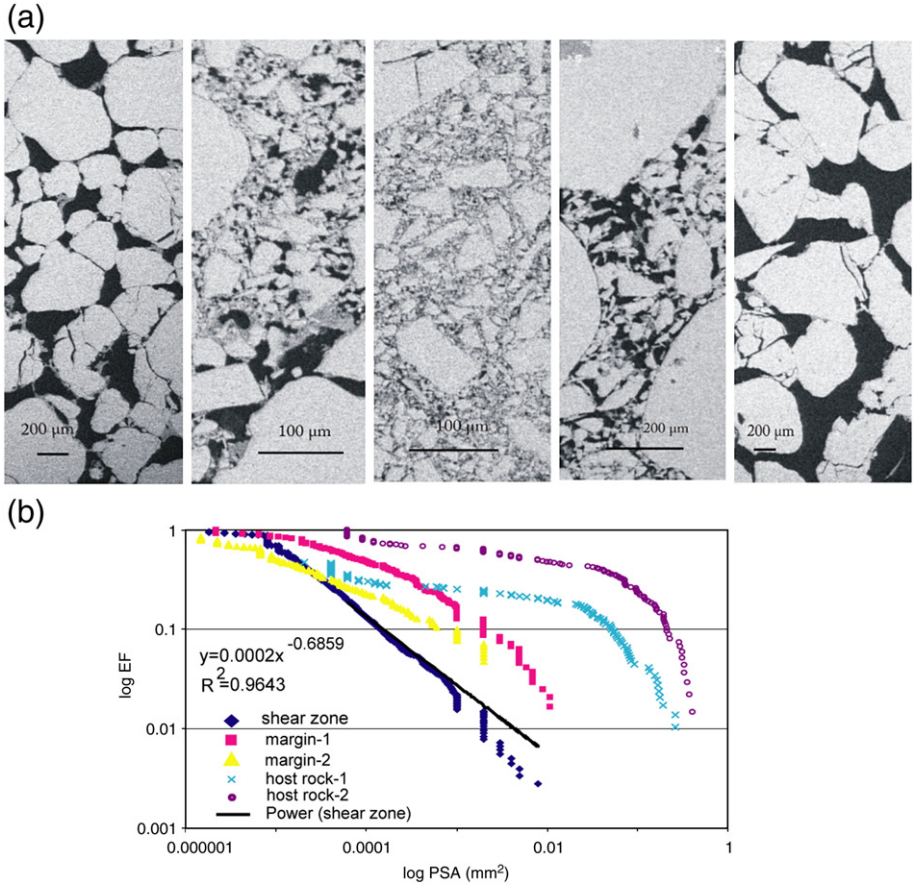

Fig. 13. (a) BSE images from thin section WK-7 (Sinai, Egypt); which presents a more compacted part in the centre of the shear zone and two margins (comparable to upper and lower margins in ring-shear result) and hosts (comparable to top and bottom layers). The shear zone can be considered as sharp boundary shear zone. (b) Grain size analysis of the thin section, which presents the grain size reduction from hosts to the shear zone; Note to the power-law fit to the shear zone with a low D value.

et al., 1999). The Nubian sandstone contains more than 90% quartz. The Tayiba fault has a throw of 120–150 m, whereas the deformation bands show throws of around 1 cm. The maximum burial depth during the formation of these structures is almost 1.5 km (Sharp, personal communication). However, a somewhat shallower depth is possible since the region was partly unroofed during progressive regional rifting.

Grain flaking is the dominant grain breakage mechanism in Corsica-3 (Fig. 11a and b), as seen by larger grains surrounded by a very fine-grained matrix in the deformation band. The band is dominated by two grain sizes and contains significant porosity. On the contrary, in TM-4 from Sinai, both flaking and splitting of grains are observed. The combination of flaking and splitting results in a few larger grains surrounded by a finer-grained matrix with a very heterogeneous grain size (Fig. 12a and b). Based on particle size analysis, the shear zones in the Corsica-3 and TM-4 are comparable to the diffuse boundary shear zones from the ring-shear experiments (Figs. 11a and 12a). WK-7 is zoned (Fig. 13a) and with a sharp boundary to the host sandstone. The core contains some smaller particles surrounded by a heterogeneous matrix, which is characteristic for combined flaking and dominant grain splitting, and the porosity is very low. The marginal zones contain larger particles but otherwise a matrix similar to the core. In this case the porosity is significantly higher. Study of the BSE images suggests that splitting is more pronounced than flaking. Grain size analysis of WK-7 (Fig. 13b) confirms the presence of a zoned shear zone with a central part of maximum grain size reduction, i.e. similar to the sharp boundary shear zone from ring-shear experiments. Besides, the grain size analysis of the shear zone from the thin sections show a power law distribution with low D values that, when compared with experimental shear zones, fits a pattern of gradual increase from 1.4 to 1.5 with higher stress (increasing burial depth and displacement).

When comparing the three examples of deformation bands, there seems to be an effect of burial depth. Near-surface faulting, as exemplified by Corsica-3, is dominated by flaking. At significant depth, represented by TM-4 and WK-7, grain splitting becomes pronounced and contributes in combination with flaking to significant grain size reduction. However, TM-4 and WK-7, which are from the same site, show clear differences. TM-4 is a diffuse boundary deformation band without zonation whereas WK-7 is a sharp boundary band that is zoned. As regards porosity, the band in TM-4 can be compared with the marginal zones of WK-7. Such differences could be explained by, for example, different burial depth during formation, since the region has experienced progressive unroofing, or by differences in shear or localization processes, or the velocity of deformation might explain the difference between WK-7 and TM-4. We return to this discussion below.

7. Discussion

There are limitations in the ring-shear experiments that have an impact on their value for comparison with deformation bands and faulted sandstone in nature. For example, the initiation of the shear zone is along a predefined plane, there is limited thickness of the confined sample inside the rings that hampers shear zone widening, and no cement is present contrary to the general observations from reservoir sandstones.

In the following, we first address the types of shear zones and the importance of grain characteristics identified in the experiments, before comparing the experimental shear zones with natural deformation bands. The latter is crucial in order to validate the experimental results before applying such results in reservoir models. According to the experiments reported here, the normal stress is the key factor that influences the type and thickness of shear zone, and the initial grain size is a subordinate factor. We conclude with a general discussion of grain size distribution, deformation mechanisms and porosity that can be expected in deformed sand and sandstone from different burial depths.

7.1. Formation of different type of shear zones

Two types of shear zones were observed in our experiments; (i) *diffuse boundary shear zones* and (ii) *sharp boundary shear zones*. Diffuse shear zones were also reported by Mandl et al. (1977) and Agung et al. (2004) who produced layered shear zone structures in both drained and undrained ring-shear tests at low normal stresses. Agung et al. (2004) divided the shear zone into three layers: The compacted core and the adjacent zones above and below the core. The sharp boundary shear zones produced in the current experiments are previously unreported from ring-shear experiments run on natural porous sand but they have been reported from the experiments on crushed granite (Beeler et al., 1996; Scruggs and Tullis, 1998). They are similar to the zoned deformation bands presented by Gabrielsen and Aarland (1990). They appear at higher levels of normal stress, as illustrated by experiments RT09 (Fig. 3b) and RT10 and are comparable with deeper burial depths as shown by the natural deformation band in WT-7 (Fig. 13) and also at high shear displacements according to the observations from experiment RT04.

Shear displacement affects the deformation mechanism. Fracturing of the grains becomes more pronounced with increased rotation in the experiments at 5 MPa (e.g. experiment RT04). At the same time the shear zone becomes more localized and strain hardened (Fig. 5a). This development can be directly linked to the formation of a sharp boundary shear zone (for example in RT04). In more detail, deformation progresses from the first part of the post-yield to the second part, representing a switch from early strain softening probably caused by crushing of the grains by either flaking or splitting in the yield stage, to strain hardening related to interlocking of the crushed grains in the shear zones followed by shear localization (Fig. 5a, b). At higher normal stress (20 MPa), the yield strength increases to more than 10 MPa (RT09 and RT10). In this condition, the mode of grain breakage is dominated by splitting rather than flaking of the grains, which leads to more compaction in the shear zone, seen as particle size and porosity reduction. The shear zone at this high normal stress (20 MPa) can be defined as a sharp boundary shear zone with a pronounced shear zone in the middle (Fig. 2b).

7.2. Effect of grain characteristics on deformation

Investigating the effect of grain size on frictional behavior of the sand (Fig. 7a) shows that initial grain size has no influence on the deformation behavior at 5 MPa normal stresses. According to Kjelstad et al. (2002), at normal stresses higher than 5 MPa, the strength values of initially loose sands are very similar for coarse-, medium-, and fine-grained mono-quartz sand. On the contrary, the effect of grain angularity and Particle Size Distribution (PSD) is important for the deformation of granular materials, as documented by Mair and Fyre (2002). They show that frictional strength and stability of a granular shear zone are sensitive to grain shape and Particle Size Distribution (PSD) during shear zone evolution. The impact is identified for different level of stress (5–25 MPa).

7.3. Comparison of experimental shear zones and natural deformation bands

The shear zones of the ring-shear experiments have a maximum thickness of 5 mm, which is approximately similar to that found for natural deformation bands, but the ring-shear experiments result in higher displacements (Fig. 10). Increasing the normal stress in the experiments (similar to burial depth in natural examples) leads to thinning of the shear zone and localization of strain. In this light, the high-displacement experimental shear zones can also be considered as analogues to sheared sand and sandstone in the core of faults. In the comparison of deformation bands sampled in sandstone from Corsica and Sinai with the experimental shear zones, it becomes clear that the experimental shear zones do not perfectly reproduce the natural examples. This can mostly be ascribed to the presence of cement in reservoir sandstone and the space restrictions imposed by the ring-shear apparatus.

Evidence of grain reorganization and flaking similar to sample Corsica-3, reveals shallow cataclasis at less than 1 km depth and favors the formation of diffuse boundary shear zones. Flaking of sand grains has also been observed in poorly consolidated sand in the Rio Grande Rift (Rawling and Goodwin, 2003). With increasing burial depth, our observations indicate that grains start to break by splitting rather than flaking, thereby promoting cataclasis (TM-4). At higher stress levels, sharp boundary shear zones form. At this stage, the deformation mechanism transgresses from predominantly flaking to predominantly splitting of the grains (e.g. the shear zone from sample WK-7 formed at about 1.5 km depth). Furthermore, grain size analyses of shear zones from the thin section show a power law distribution with low D values for all the three natural samples that fit a pattern of gradual increase of the dimension with higher stress (increasing burial depth and displacement).

7.4. Grain size distribution and deformation mechanism

In the present study, using different sands (quartz arenite) in the drained ring-shear experiments when (unlike the natural cases) there is no chemical alteration in the sample during deformation, the deformation of quartz and feldspar grains are similar at low normal stress (5 MPa, less than 1 km burial depth). Hence, grains have been broken mostly by flaking of the grain surfaces by abrasion, resulting in a low fractal dimension (1.4). With increasing burial depth (20 MPa, or more than 2 km burial depth), grains start to split. The change in the mode of fracturing from flaking to splitting increases the fractal dimension gradually. We conclude that the burial depth (normal stress in our experiments) and applied shear displacement are two significant factors influencing grain crushing and the resulting D values. Comparison of our results with previous studies reveals that even at 20 MPa normal stresses we do not reach the steady state particle size distribution ($D \sim 2.58$). We consider the mechanism of deformation at shallow depth/low level of stress to be dominated by reorganization, rolling and

flaking and minor splitting of the grains. This mechanism causes rough grain surfaces at the margins and within the shear zones, and produces a matrix of elongated grains surrounding surviving coarser grains. At deeper or at higher levels of stress the mode of fracturing transgresses from predominantly flaking to predominantly grain splitting, causing lower porosity values and increased particle size reduction.

Rawling and Goodwin (2003) assumed that their samples at low confining pressure had not reached a steady-state particle size distribution (characterized low D values of 1.7–2.1). Hence, with further deformation the particle size distribution would change, perhaps resulting in higher D values. Further, this transition results in a slow increase in the D values.

At higher confining pressure and burial depth, the relative size of the individual grains becomes an important factor influencing the grain fracturing (Sammis et al., 1987). At yet higher confining pressure, the third process of Blenkinsop (1991); (particle size reduction due to cataclasis); is responsible for fragmentation which is the development of cataclasis in a process of selective fracturing of relatively larger particles. This may also operate during localization and faulting.

A power-law gives the best fit for particle size area distribution of shear zones in this study. The power-law distribution is the only distribution that does not include a characteristic length scale. Thus it must be applicable to scale-invariant phenomena (Mandelbrot, 1982; Turcotte, 1997). A fractal distribution requires the number of objects larger than a specified size to have a power-law dependence on the size (Turcotte, 1997).

The power-law distributions, which fall within the limits of non-integer/fractional dimensions, i.e., $0<D<3$, can be defined as fractals and clearly scale-invariant (Turcotte, 1997). The power dimensions from both the experiments and natural examples are very low and so they might be considered as fractional dimensions. Since the dominant flaking at low stress levels creates angular and non-similar grains, the term self-affine might fit to this type of fractal. The power-law distribution is a non-linear relationship, which reveals that the obtained particle size distribution in the shear zones can be expressed by other factors, such as burial depth, stress levels at the time of deformation and strength of the grains.

8. Conclusions

Shear zones created in ring-shear experiments have been studied and compared with natural examples. Based on this study, the shear zone has been divided into three layers; (i) the “top layer”, representing the upper part; (ii) the “shear zone” or the middle part; and (iii) the “bottom layer” or the lower part of the section. The particle size distribution analysis shows that particle sizes are smaller in the middle part of the shear zone. The thin sections also show the development of two end-member types of shear zones: (a) Shear zones with diffuse boundaries formed at low levels of stress, and (b) Shear zones with sharp boundaries formed at higher levels of stress. We conclude that the burial depth (normal stress in our experiments) and the applied shear displacement are two significant factors influencing grain crushing and the resulting D values. We consider the mechanism of deformation at shallow depth/low level of stress to be dominated by reorganization, rolling and flaking of the grains. This mechanism causes rough surfaces of grains at the margins and within the shear zones. At higher burial depths or levels of stress the fracturing mode transgresses from predominantly flaking to predominantly grain splitting, causing lower porosity values and higher particle size reduction. Further, this transition result in a slow increase in the grain size-distribution D values.

We conclude that initial grain size has no influence on the deformation behavior of the sand at 5 MPa normal stresses. Comparison of experimental shear zones with the natural ones shows similar thickness but different displacements. Furthermore we presented comparable experimental shear zones to the natural examples.

Acknowledgments

The ring-shear experiments were carried out as part of the Fault Seal Project managed by the ”Norwegian Geotechnical Institute” (NGI) between 2003 and 2006, which was supported by NGI, The Norwegian Research Council (NRC), Norsk Hydro ASA, and Total. The permission to use data and publish the results is greatly appreciated. Professor Knut Bjørlykke (University of Oslo) advised in the course of the project. We appreciate the experimental work that has been carried out by Ra Cleave, Elin Skurtveit, Lars Grande and Trude Ørbech at NGI. Thanks go to Egil Erichsen for help with the SEM analyses and also to Brian Anthony Farrelly for his great help and kindness. This study was completed in the frame of Fault Facies Project at the Centre for Integrated Petroleum Research, University of Bergen, and supported by NRC, Statoil, Conoco-Philips, and Statoil-Vista.

References

Agung, M.W., Sassa, K., Fukuoka, H., Wang, G., 2004. Evolution of shear-zone structure in undrained ring-shear tests. Landslides 1, 101–112.

Antonellini, M., Aydin, A., 1999. Outcrop-aided characterization of a faulted hydrocarbon reservoir: Arroyo Grande Oil Field, California,

USA. Faults and subsurface fluid flow in the shallow crust. American Geophysical Union 113, 7–26.
Aydin, A., 1978. Small faults formed as deformation bands in sandstone. Pure and Applied Geophysics 116, 913–930.
Aydin, A., Borja, R.I., Eichhubl, P., 2006. Geological and mathematical framework for failure modes in granular rock. Journal of Structural Geology 28, 83–98.
Beach, A., Welbon, A.I., Brockbank, P.J., McCallum, J.E., 1999. Reservoir damage around faults: outcrop examples from the Suez rift. Petroleum Geoscience 5 (2), 109–116.
Beeler, N.M., Tullis, T.E., Blanoped, M.L., Weeks, J.D., 1996. Frictional behaviour of large displacement experimental faults. Journal of Geophysical Research 101 (B4), 8697–8715.
Bishop, A.W., Green, G.E., Garga, V.K., Andersen, A., Brown, J.D., 1971. A new ring-shear apparatus and its application to the measurement of residual strength. Geotechnique 21 (1), 273–328.
Blenkinsop, T.G., 1991. Cataclasis and processes of particle size reduction. PAGEOPH 136 (1).
Clausen, J.A., Gabrielsen, R.H., 2002. Parameters that control the development of clay smear at low stress states: an experimental study using ring-shear apparatus. Journal of Structural Geology 24 (10), 1569–1586.
Cuisiat, F., Skurtveit, E., 2006. Large strain testing of fault seals. Final Report on Fault Seal Project, NGI Repot No 2001288-3.
Fossen, H., Hesthammer, J., 2000. Possible absence of small faults in the Gullfaks Field, northern North Sea. Journal of Structural Geology 22 (7), 851–863.
Fossen, H., Schultz, R.A., Shipton, Z., Mair, K., in press. Deformation bands in sandstone — a review. Journal of the Geological Society (London), 164.
Fowles, J., Burley, S., 1994. Textural and permeability characteristics of faulted, high porosity sandstones. Marine and Petroleum Geology 11 (5).
Gabrielsen, R.H., Aarland, R.K., 1990. Characteristics of pre-syn-consolidation structures and tectonic joints and microfaults in fine- to medium-grained sandstones. Rock Joints. Balkema, Amsterdam, pp. 45–50.
Garga, V.K., Sendano, J.I., 2002. Steady state strength of sands in a constant volume ring shear apparatus. Geotechnical Testing Journal 25 (4), 414–421.
Hvorslev, M.J., 1939. Torsion shear tests and their place in the determination of the shearing resistance of soils. Proc. Am. Soc. Test. Mater., vol. 39, pp. 999–1022.
Kjelstad, A., Chuhan, F., Høeg, K., Bjørlykke, K., 2002. Cataclastic shear band formation in sands at high stresses: An analogue experimental model and its relevance for faults in sedimentary basins. PhD Thesis, University of Oslo.
Lothe, A.E., Bjørnevoll Hagen, N., Gabrielsen, R.H., Larsen, B.T., 2002. An experimental study of the texture of deformation bands: effects on porosity and permeability of sandstones. Petroleum Geoscience 8, 195–207.
Main, I., Mair, K., 2001. Experimental constraints on the mechanical and hydraulic properties of deformation bands in porous sandstones: a review. In: Holdsworth, R.E, Strachan, R.A., Magloughlin, J.F., Knipe, R.J. (Eds.), The Nature and Tectonic Significance of Fault Zone Weakening. Geological Society, London, Special Publication, vol. 186, pp. 43–63.
Mair, K., Fyre, K.M., 2002. Influence of grain characteristics on the friction of granular shear zones. Journal of Geophysical Research 107 (B10).
Mair, K., Main, I., 2000. Sequential growth of deformation bands in the laboratory. Journal of Structural Geology 22, 25–42.
Mandelbrot, B.B., 1982. The Fractal Geometry of Nature. Freeman, San Fransisco.
Mandl, G., de Jong, L.N., Maltha, A., 1977. Shear zones in granular material. Rock Mechanics 9, 95–144.
Marone, C., Scholz, C.H., 1989. Particle-size distribution and microstructures within simulated fault gouge. Journal of Structural Geology 11 (7), 799–814.
Ngwenya, B.T., Kwon, O., et al., 2003. Permeability evolution during progressive development of deformation bands in porous sandstones. Journal of Geophysical Research 108 (B7), 2343.t1 doi:10.1029/2002JB001854.
Rawling, G.C., Goodwin, L.B., 2003. Cataclasis and particulate flow in faulted, poorly lithified sediments. Journal of Structural Geology 25 (3), 317–331.
Sammis, C., King, G., Biegel, R., 1987. The kinematics of gouge deformation. PAGEOPH 125 (5).
Sassa, K., Fukuoka, H., Wang, G., Ishikawa, N., 2004. Undrained dynamic-loading ring-shear apparatus and its application to landslide dynamics. Landslides 1, 7–19.
Schultz, R.A., Siddharthan, R., 2005. A general framework for the occurrence and faulting of deformation bands in porous granular rocks. Tectonophysics 411, 1–18.
Scruggs, V.J., Tullis, T.E., 1998. Correlation between velocity dependence of friction and strain localization in large displacement experiments on feldspar, muscovite and biotite gouge. Tectonophysics 295, 15–40.
Sperrevik, S., Gillespie, P.A., Fisher, Q.J., Halvorsen, T., Knipe, R.J., 2002. Empirical estimation of fault rock properties. In: Koestler, A.G., Hunsdale, R. (Eds.), Hydrocarbon Seal Quantification. Norwegian Petroleum Society (NPF), Special Publication, vol. 11, pp. 109–125.
Turcotte, D.L., 1997. Fractals and Chaos in Geology and Geophysics. Cambridge University Press.
Underhill, J.R., Woodcock, N.H., 1987. Faulting mechanisms in high-porosity sandstones; New Red Sandstone, Arran, Scotland. In: Jones, M.E., Preston, R.M.F. (Eds.), Deformation of Sediments and Sedimentary Rocks. Geological Society Special Publication, vol. 29, pp. 91–105.
Zhang, S., Tullis, T.E., 1998. The effect of fault slip on permeability and permeability anisotropy in quartz gouge. Tectonophysics 295 (1-2), 41–52.
Zhu, W., Wong, T., 1997. The transition from brittle faulting to cataclastic flow. Journal of Geophysical Research 102 (B2), 3027–3041.